Proceedings of the 10th Brazilian Congress of Thermal Sciences and Engineering -- ENCIT 2004
Braz. Soc. of Mechanical Sciences and Engineering -- ABCM, Rio de Janeiro, Brazil, Nov. 29 -- Dec. 03, 2004

Paper CIT04-0799

SURFACE TEMPERATURE EFFECTS IN LOW-DENSITY FLOW OVER FLAT-NOSE BODIES AT HYPERSONIC SPEED. PART I: FLOWFIELD STRUCTURE

Wilson F. N. Santos
National Institute for Space Research
Combustion and Propulsion Laboratory
12630-000 Cachoeira Paulista, SP, Brazil
wilson@lcp.inpe.br

Abstract. *Hypersonic flow past flat-nose leading edges at zero incidence is investigated for a range of body surface temperature from 440 to 1100 K.. The work is motivated by interest in assessing the overall performance of flat-nose leading edges in order to consider them as possible candidates for blunting geometries of hypersonic configurations. The Direct Simulation Monte Carlo (DSMC) method has been employed in order to examine the flowfield structure around these leading edges. A very detailed description of the primary flow property behavior immediately adjacent to the body surface has been presented by a numerical method that properly accounts for non-equilibrium effects arising near the leading edge and that are especially important at high Mach number. The results presented highlight some significant differences on the flowfield properties due to variations on the nose thickness and on the wall temperature. It is found that the upstream effects have different influence on velocity, density, pressure and temperature along the stagnation streamline ahead of the leading edges.*

Keywords. *DSMC, hypersonic flow, rarefied flow, blunt leading edge, sharp leading edge.*

1. Introduction

An efficient design of future airbreathing hypersonic vehicle will depend on high-lift low-drag configurations in order to overcome the aerodynamic forces involved in high-speed flight. For this purpose, waveriders, first conceived by Nonweiler (1959), have been considered as one of the promising vehicle concepts under consideration. Waveriders are vehicles designed so that the bow shock is everywhere attached to the sharp leading edge. Because of the shock wave is attached to the leading edge of the vehicle, the upper and lower surface of the vehicle can be designed separately. In this respect, the shock wave acts as a barrier in order to prevent spillage of the high pressure airflow from the lower side of the vehicle to the upper side, resulting in a high-pressure differential and enhanced lift.

Nevertheless, actual flight vehicle will include some degree of bluntness, either dictated by manufacturing requirements or by heating requirements. The latter is especially important given that heating rate on rounded edges scales inversely with the square root of the stagnation point radius, so that there is an unavoidable compromise between aerodynamic performance and heating survivability. Therefore, designing a hypersonic vehicle leading edge involves a tradeoff between making the leading edge sharp enough to obtain acceptable aerodynamic and propulsion efficiency and blunt enough to reduce the aerodynamic heating in the stagnation region.

Certain classes of non-circular shapes may provide the required bluntness with smaller shock separation than round leading edges, which scales with the radius of curvature, thus allowing manufacturing, and ultimately heating control, with reduced departures from ideal aerodynamic performance. The idea that such would be possible is based on the work of Reller (1957) who has presented a method of designing low heat transfer bodies. The method is devised on the premise that the rate of heat transfer to the nose will be low if the local velocity is low, while the rate of heat transfer to the afterbody will be low if the local density is low. A typical body that results from this design method consists of a flat nose followed by a highly curved, but for the most part slightly inclined, afterbody surface.

Santos (2003) has investigated the sensitivity of the stagnation point heating and total drag to shape variations of such leading edges. The emphasis of the work was to compare flat-nose leading edges with round leading edges (circular cylinder) in order to determine which geometry would be better suited as a blunting profile in terms of stagnation point heating and total drag coefficient. His analysis showed that circular cylinder still provided smaller stagnation point heating than flat-nose leading edges under the range of conditions investigated. Nonetheless, flat-nose leading edges yielded lower total drag and much smaller shock standoff distance than the circular cylinder.

The present account extends the analysis presented by Santos (2003) by examining computationally the flowfield structure for a family of these flat-nose contours with great deal of emphasis placed on the body surface temperature effects. The investigation has been made for four different wall temperatures but with the same freestream conditions.

The present study is focused on the low-density region in the upper atmosphere, where the non-equilibrium conditions are such that traditional CFD calculations are inappropriate to yield accurate results. In such a circumstance, the DSMC method will be employed to calculate the rarefied hypersonic two-dimensional flow on the leading edge shapes.

2. Body Shape Definition

In dimensionless form, the contour that defines the shape of the afterbody surface is given by,

$$\bar{x} = \int_{\bar{y}=1}^{\bar{y}=\bar{y}_{\max}} \sqrt{\bar{y}^k - 1}\, d\bar{y} \tag{1}$$

where $\bar{x} = x/y_{nose}$ and $\bar{y} = y/y_{nose}$.

The blunt shapes are modeled by assuming a sharp leading edge of half angle θ with a circular cylinder of radius R inscribed tangent to the wedge. The blunt shapes, inscribed between the wedge and the cylinder, are also tangent to them at the same common point where they have the same slope angle. The circular cylinder diameter provides a reference for the amount of blunting desired on the leading edges. It was assumed a leading edge half angle of 10 deg, a circular cylinder diameter of 10^{-2}m and flat-nose thickness t/λ_∞ of 0.01, 0.1 and 1, where $t = 2y_{nose}$ and λ_∞ is the freestream mean free path. Figure (1a) illustrates this construction for the set of shapes investigated. From geometric considerations, the exponent k in Eq. (1) is obtained by matching slope on the wedge, circular cylinder and on the body shapes at the tangency point. For dimensionless thicknesses of 0.01, 0.1 and 1, the exponent k corresponds to 0.501, 0.746 and 1.465, respectively. The common body height H and the body length L are obtained in a straightforward manner. It was assumed that the leading edges are infinitely long but only the length L is considered, since the wake region behind the leading edges is not of interest in this investigation.

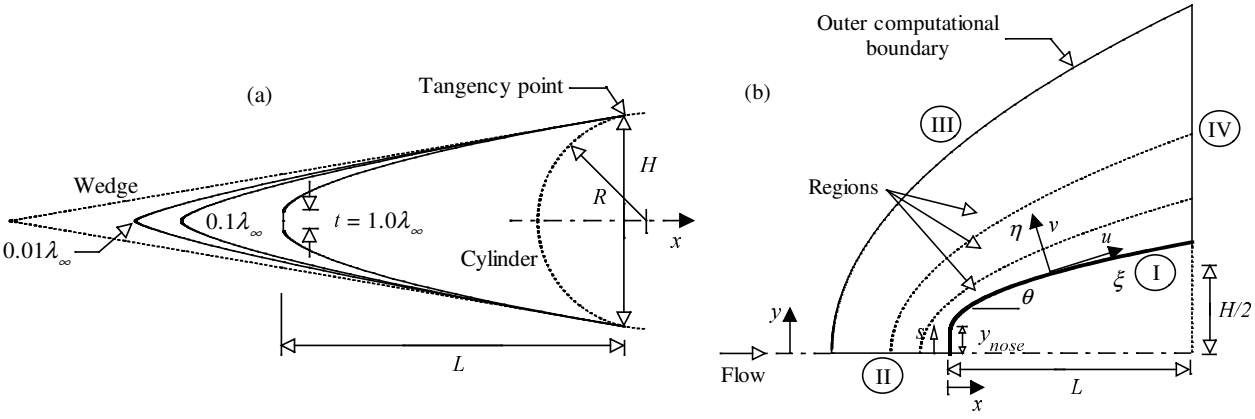

Figure 1: Drawing illustrating (a) the leading edge shapes and (b) the computational domain.

3. Computational Method and Procedure

The most successful numerical technique for modeling complex transitional flows has been the Direct Simulation Monte Carlo (DSMC) method (Bird, 1994). The DSMC method simulates real gas flows with various physical processes by means of a huge number of modeling particles, each particle represents a fixed number of real gas molecules. In the DSMC model, the particle evolution is divided into two independent phases during the simulation; the movement phase and the collision phase. In the movement phase, all particles are moved over distances appropriate to a short time interval, time step, and some of them interact with the domain boundaries in this time interval. Particles that strike the solid wall would reflect according to the appropriate gas-surface interaction model, specular, diffusive or a combination of these. In the collision phase, intermolecular collisions are performed according to the theory of probability without time being consumed. In this context, the intermolecular collisions are uncoupled to the translational molecular motion over the time step used to advance the simulation. Time is advanced in discrete steps such that each step is small in comparison with the mean collision time. The simulation is always calculated as unsteady flow. However, a steady flow solution is obtained as the large time state of the simulation.

The molecular collisions are modeled using the variable hard sphere (VHS) molecular model (Bird, 1981) and the no time counter (NTC) collision sampling technique (Bird, 1989). The energy exchange between kinetic and internal modes is controlled by the Borgnakke-Larsen statistical model (Borgnakke and Larsen, 1975). Simulations are performed using a non-reacting gas model consisting of two chemical species, N_2 and O_2. Energy exchanges between the translational and internal modes, rotational and vibrational, are considered. Relaxation collision numbers of 5 and 50 were used for the calculations of rotation and vibration, respectively.

In order to easily account for particle-particle collisions, the flowfield is divided into an arbitrary number of regions, which are subdivided into computational cells. The cells are further subdivided into subcells. The cell

provides a convenient reference sampling of the macroscopic gas properties, while the collision partners are selected from the same subcell for the establishment of the collision rate.

The computational domain used for the calculation is made large enough so that body disturbances do not reach the upstream and side boundaries, where freestream conditions are specified. A schematic view of the computational domain is depicted in Fig. (1b). Side I is defined by the body surface. Diffuse reflection with complete thermal accommodation is the condition applied to this side. Advantage of the flow symmetry is taken into account, and molecular simulation is applied to one-half of a full configuration. Thus, side II is a plane of symmetry. In such a boundary, all flow gradients normal to the plane are zero. At the molecular level, this plane is equivalent to a specular reflecting boundary. Side III is the freestream side through which simulated molecules enter and exit. Finally, the flow at the downstream outflow boundary, side IV, is predominantly supersonic and vacuum condition is specified (Guo and Liaw, 2001). At this boundary, simulated molecules can only exit.

Application of a numerical method to solve practical problems requires a reliable way in order to estimate the accuracy of the solution. The numerical accuracy in DSMC method depends on the cell size chosen, on the time step as well as on the number of particles per computational cell. In the DSMC algorithm, the linear dimensions of the cells should be small in comparison with the scale length of the macroscopic flow gradients normal to streamwise directions, which means that the cell dimensions should be of the order of or smaller than the local mean free path (Alexander et al., 1998 and Alexander et al., 2000). The time step should be chosen to be sufficiently small in comparison with the local mean collision time (Garcia and Wagner, 2000, and Hadjiconstantinou, 2000). In general, the total simulation time, discretized into time steps, is identified with the physical time of the real flow. Finally, the number of simulated particles has to be large enough to make statistical correlations between particles insignificant.

These effects were investigated in order to determine the number of cells and the number of particles required to achieve grid independence solutions. Grid independence was tested by running the calculations with half and double the number of cells in ξ and η directions (see Fig. (1b)) compared to a standard grid. Solutions (not shown) were near identical for all grids used and were considered fully grid independent.

The freestream and flow conditions used in the present calculations are those given by Santos (2003) and summarized in Tab. (1). The gas properties considered in the simulation are those given by Bird (1994) and shown in Tab. (2). The freestream velocity V_∞, assumed to be constant at 3.56 km/s, corresponds to a freestream Mach number M_∞ of 12. In order to simulate the surface temperature effects, the wall temperature T_w is assumed constant at 440, 660, 880 and 1100 K, which correspond to 2, 3, 4 and 5 times the freestream temperature, respectively.

Table 1: Freestream Conditions

Temperature T_∞ (K)	Pressure p_∞ (N/m^2)	Density ρ_∞ (kg/m^3)	Number density n_∞ (m^{-3})	Viscosity μ_∞ (Ns/m^2)	Mean free path λ_∞ (m)	Velocity V_∞ (m/s)
220.0	5.582	8.753×10^{-5}	1.8209×10^{21}	1.455×10^{-5}	9.03×10^{-4}	3560

Table 2: Gas Properties

	Mole fraction X	Molecular mass m (kg)	Molecular diameter d (m)	Viscosity Index ω
O_2	0.237	5.312×10^{-26}	4.01×10^{-10}	0.77
N_2	0.763	4.65×10^{-26}	4.11×10^{-10}	0.74

The overall Knudsen number Kn_t, defined as the ratio of the freestream mean free path λ_∞ to the leading edge thickness t, corresponds to 1, 10 and 100 for leading edge thickness t/λ_∞ of 1, 0.1 and 0.01, respectively. The Reynolds number Re_t covers the range from 0.193 to 19.3, based on conditions in the undisturbed stream with leading edge thickness t as the characteristic length.

4. Computational Results and Discussions

Having computed flowfield properties over a wide range of input conditions and simulation parameters, it proved instructive to summarize the major features of the results. In this scenario, the purpose of this section is to discuss and to compare differences in the flowfield properties due to variations on the leading edge thickness and on the wall temperature. The flowfield properties of particular interest in the transitional flow regime are velocity, density, pressure and temperature.

4.1. Velocity Profile

Normal velocity profiles along the stagnation streamline and their dependence on the body surface temperature are illustrated in Figs. (2a), (2b) and (2c) for leading edge thickness t/λ_∞ of 0.01, 0.1 and 1, which correspond to Kn_t of 100,

10 and 1, respectively. Each profile has been taken through cell centroids that lie very close to the stagnation line, and therefore can be considered as being along the stagnation streamline. In this set of figures, the velocity ratio stands for the normal velocity v normalized by the freestream velocity V_∞, and the dimensionless height is the distance upstream the leading edges along the body normal (η) direction (see Fig. (1b)) normalized by the freestream mean free path λ_∞.

According to these figures, it is seen that the leading edge thickness as well as the wall temperature influences the flowfield far upstream. This domain of influence increases with increasing both the leading edge thickness and the wall temperature. The leading edge thickness effect results from the upstream diffusion of particles that are reflected from the nose of the leading edge. Consequently, blunting the nose of the body (increasing t) leads to significantly larger disturbance upstream of the body. In addition, the wall temperature effect results from particles reflecting from hotter surface with greater energies that diffuse further upstream. For instance, the upstream disturbance for a velocity reduction of 1% ($v/V_\infty = 0.99$) is around $2.07\lambda_\infty$, $2.65\lambda_\infty$ and $4.78\lambda_\infty$ for cases $t/\lambda_\infty = 0.01$, 0.1 and 1, respectively, with wall temperature of 440K. However, it changes to around $2.82\lambda_\infty$, $3.41\lambda_\infty$ and $5.28\lambda_\infty$ for cases $t/\lambda_\infty = 0.01$, 0.1 and 1, respectively, and wall temperature of 1100K.

Variation of the tangential velocity u in the body normal direction is depicted in Fig. (3) as a function to the wall temperature for the $Kn_t = 1$ case. In an effort to emphasize points of interest, this set of plots presents data at three afterbody stations that correspond to body slope angle of 80, 40 and 20 degrees. Of great significance in this set of figures is the slip velocity. It is seen that slip velocity slightly increases with increasing the wall temperature. It should be noted that the tangential velocity reaches the freestream limit value u_∞, represented by the dashed line, close to the body surface for the station in the vicinity of the shoulder. Because of the body curvature, u_∞ varies as a function of the body slope.

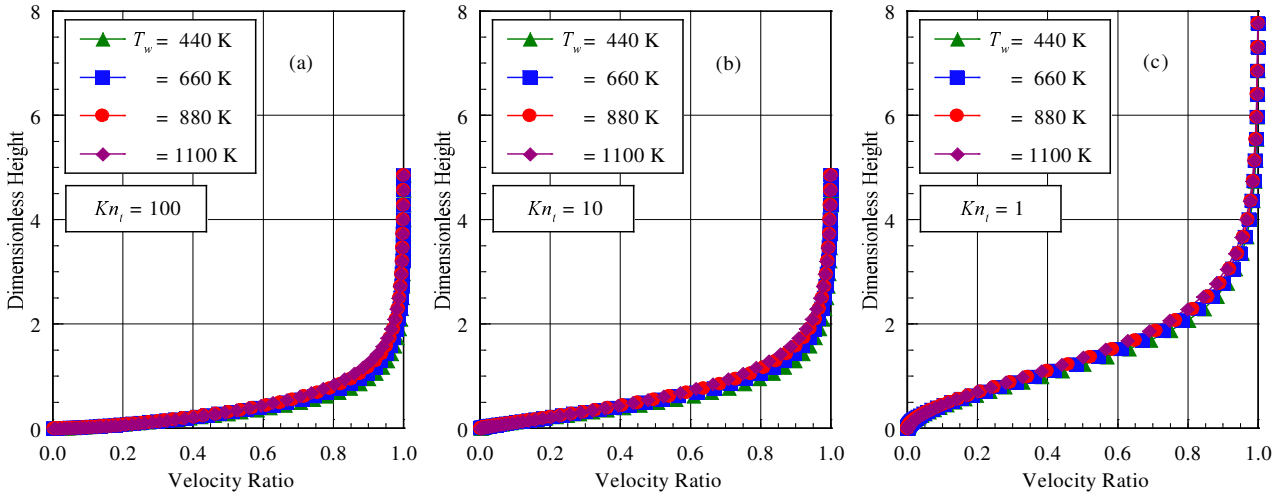

Figure 2: Normal velocity ($-v/V_\infty$) profiles along the stagnation streamline as a function of the wall temperature for leading edge thicknesses that correspond to Knudsen number Kn_t of (a) 100, (b) 10 and (c) 1.

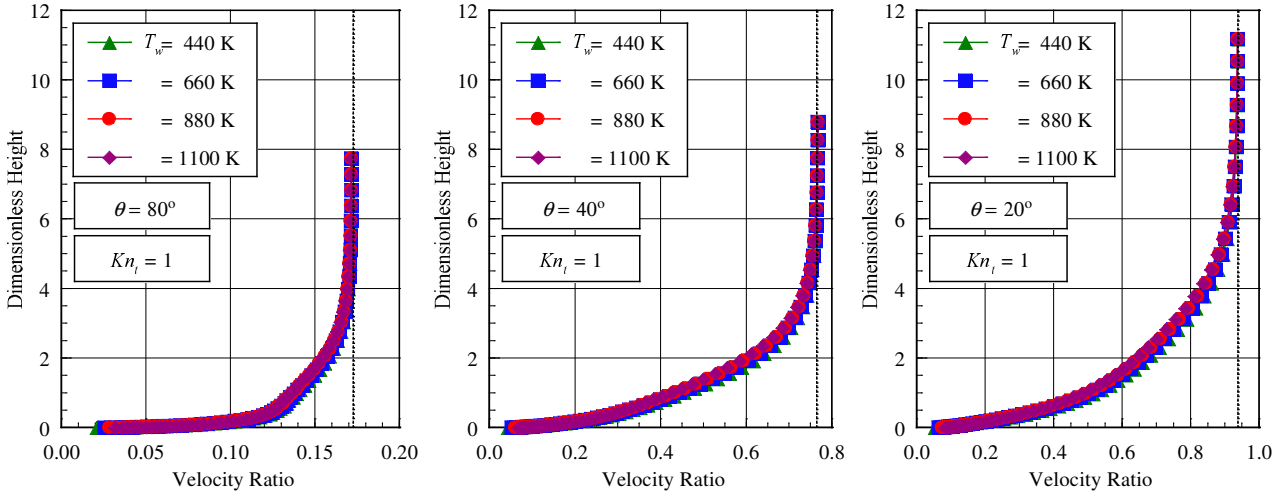

Figure 3: Tangential velocity (u/V_∞) profiles along the body normal direction as a function of the wall temperature for Knudsen number Kn_t of 1 at afterbody stations that correspond to (a) 80, (b) 40 and (c) 20 degrees.

4.2. Density Profile

Density profiles along the stagnation streamline are plotted as a function of the wall temperature in Figs. (4a), (4b) and (4c) for Kn_l of 100, 10 and 1, respectively. In this set of figures, dimensionless height is the distance in the normal body direction η normalized by λ_∞, and density ratio is the density ρ normalized by the freestream density ρ_∞.

The predictions of density for all of the leading edge thicknesses investigated show no sign of a discrete shock wave. Instead, there is a continuous rise in density from the freestream to the nose of the leading edges, rising to well above the continuum inviscid limit. As a point of reference, the Rankine-Hugoniot relations give a postshock density that corresponds to the ratio $\rho/\rho_\infty = 5.8$ for freestream Mach number of 12. Near the stagnation point ($\eta/\lambda_\infty \approx 0$), a substantial density increase occurs which is a characteristic of cold-wall entry flow (Haas and Fallavollita, 1994). In typical entry flow, the body surface temperature is low compared to the stagnation temperature. This leads to a steep density gradient near the body surface. For the present simulation, the ratio of wall temperature to stagnation temperature is from 0.07 to 0.18, which correspond to a cold-wall flow.

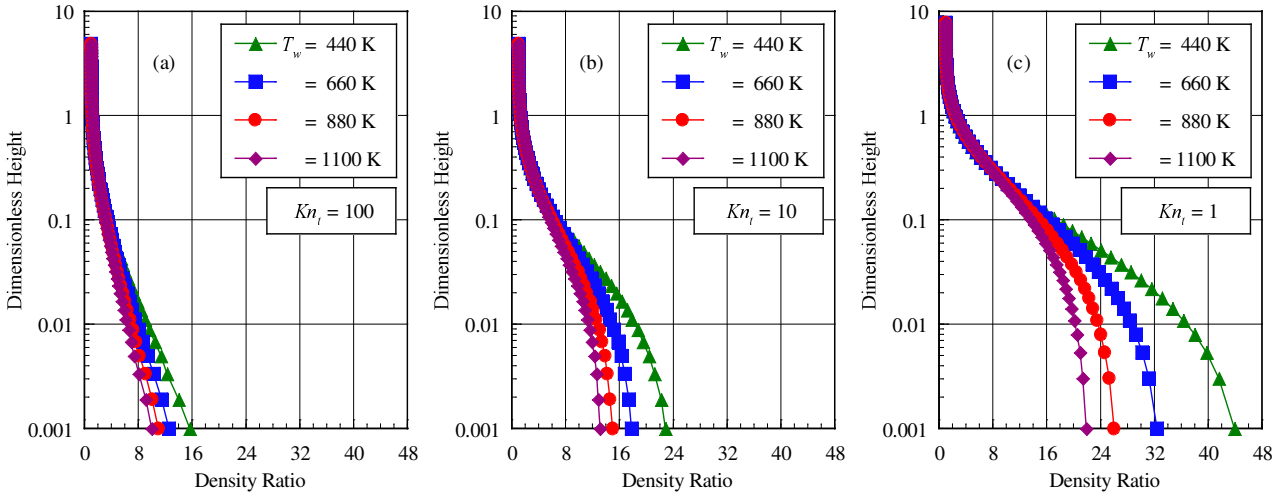

Figure 4: Density (ρ/ρ_∞) profiles along the stagnation streamline as a function of the wall temperature for leading edge thicknesses that correspond to Knudsen number Kn_l of (a) 100, (b) 10 and (c) 1.

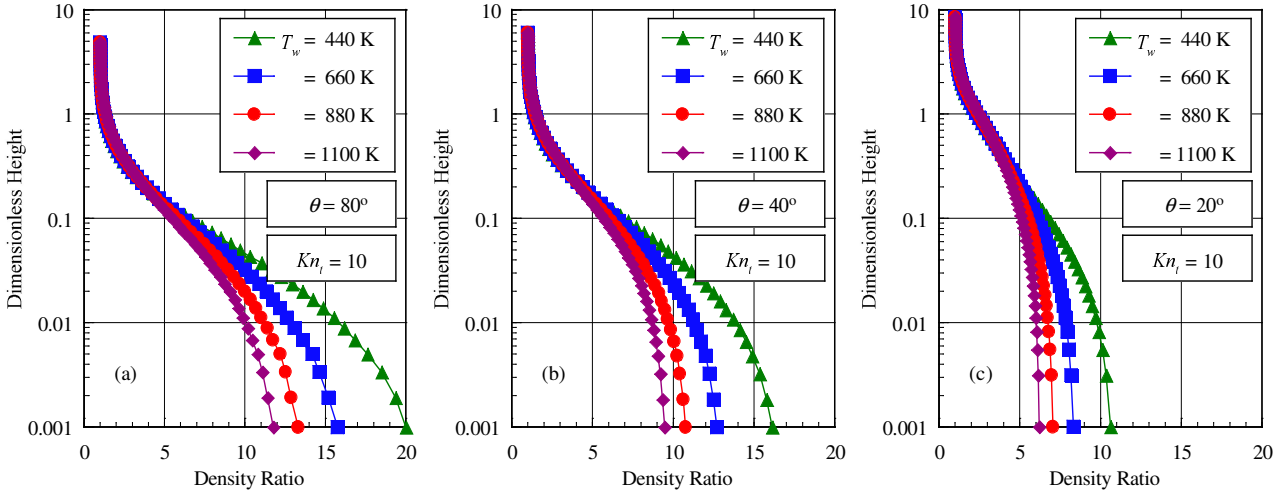

Figure 5: Density (ρ/ρ_∞) profiles along the body normal direction as a function of the wall temperature for Knudsen number Kn_l of 10 at afterbody stations that correspond to (a) 80, (b) 40 and (c) 20 degrees.

Referring to Figs. (4a) – (4c), it can be recognized that density rises gradually as the flow approaches the nose of the leading edge, indicating the diffuse nature of the shock wave, a characteristic of highly rarefied flows. As the wall temperature is increased from 440 K to 1100 K, the particles are reflected from the surface with greater energies. This leads to greater relative translational velocities and flowfield temperatures. Consequently, energetic reflections from hotter surface reduce the net buidup of particle density near the body surface. By examining the density profiles, two regions are seen; one inner region close to the stagnation point, roughly defined by $\eta/\lambda_\infty < 0.1$ and < 0.3 for $Kn_l = 100$ and 1, respectively, where variation in the wall temperature affects the density profiles, and an outer region, $\eta/\lambda_\infty > 0.1$

and > 0.3 for Kn_t = 100 and 1, respectively, where virtually no effect is detected due to the wall temperature rise. Furthermore, as the leading edge becomes flatter, the extent of the flowfield disturbances becomes much larger, as evidenced by the density profiles.

By considering free molecular flow (Bird, 1994), the density ratio at the stagnation point is equal to 13.6, 11.3, 9.9 and 9.0 for wall temperature of 440, 660, 880 and 1100 K, respectively. It may be recognized from the density distribution in Fig. (4a) that the density ratio for the Kn_t = 100 case (t/λ_∞ = 0.01 case) is approaching the free molecular value at the stagnation point. Unlike normal velocity, density has little effect on the extent of the domain of influence upstream of the body for the leading edge thicknesses investigated. Much of the density increase in the shock layer occurs after the temperature has reached its postshock value, as will be seen subsequently.

Figure (5) displays selected profiles of the local density, expressed as a ratio to the freestream value, for three stations located on the afterbody surface related to the Kn_t = 10 case (t/λ_∞ = 0.1 case). It is observed that density is affected by the wall temperature rise, as would be expected. For the station corresponding to 80 deg, Fig. (5a), the density variation is in excess of one order of magnitude for the wall temperature investigated. In this region, close to the stagnation region, the compression combined with a relatively cool wall produces a maximum density that is 20 and 12 times the freestream value for cases with wall temperature of 440 and 1100 K, respectively. Because of the expansion along the body surface, the density adjacent to the surface decreases to 11 and 6 times the freestream value for wall temperature cases of 440 and 1100 K, respectively, at the station corresponding to 20 deg, Fig. (5c), a reduction around of 50%.

4.3. Temperature Profile

Blunting the leading edge moves the shock wave created during the hypersonic flight forward and out, away from the leading edge, creating an air pocket in front of it. This strong shock wave that forms ahead of a blunt leading edge at hypersonic flow converts part of the kinetic energy of the freestream air molecules into thermal energy. This thermal energy downstream of the shock wave is partitioned into increasing the translational kinetic energy of the air molecules, and into exciting of other molecular energy states such as rotation and vibration.

Kinetic temperature profiles along the stagnation streamline are demonstrated in Figs. (6) and (7) for wall temperature cases of 440 and 1100 K, respectively. In this set of figures, temperature ratio accounts for the kinetic temperatures normalized by the freestream temperature T_∞. It is apparent from these figures that thermodynamic non-equilibrium occurs throughout the shock layer, as shown by the lack of equilibrium of the translational and internal kinetic temperatures. Thermal non-equilibrium occurs when the temperatures associated with the translational, rotational, and vibrational modes of a polyatomic gas are different.

The overall kinetic temperature shown is defined for a non-equilibrium gas as the weighted mean of the translational and internal temperature (Bird, 1994) as follows,

$$T = \frac{\zeta_T T_T + \zeta_R T_R + \zeta_V T_V}{\zeta_T + \zeta_R + \zeta_V} \tag{2}$$

where ζ is the degree of freedom, and subscripts T, R and V stand for translational, rotational and vibrational modes.

The overall kinetic temperature is equivalent to the thermodynamic temperature only under thermal equilibrium conditions. As a matter of fact, it should be noticed that the ideal gas equation of state does not apply to this temperature in a non-equilibrium situation.

Referring to Figs. (6)-(7), in the undisturbed freestream far from the body, the translational and internal temperatures have the same value and are equal to the thermodynamic temperature. Approaching the nose of the leading edge, the translational temperature rises to well above the rotational and vibrational temperatures and reaches a maximum value that is a function of the leading edge thickness as well as of the wall temperature. Since a large number of collisions is needed to excite molecules vibrationally from the ground state to the upper state, the vibrational temperature increases much more slowly than rotational temperature. Still further downstream toward the nose of the leading edge, the translational temperature decreases and reaches a value on the wall that is above the wall temperature, resulting in a temperature jump as defined in continuum formulation.

The substantial rise in translational kinetic temperature for blunt leading edges occurred before the density rise (see Fig. (4). For instance, the kinetic translational temperature reaches the maximum value around a distance of one freestream mean free path from the nose of the leading edge for the case Kn_t = 1 and T_w = 440 K, while the density ratio ρ/ρ_∞ is around 2.4 at the same station. The translational kinetic temperature rise for blunt leading edges results from the essentially bimodal velocity distribution (Liepmann et al., 1964): the molecular sample consisting of mostly undisturbed freestream molecules with the molecules that have been affected by the shock and reflected from the body. In this connection, the translational kinetic temperature rise is a consequence of the large velocity separation between these two classes of molecules.

Particular attention is paid to the translational temperature in the shock layer. In this respect, the translational temperature variation is taken normal to the body surface at afterbody stations corresponding to 80, 40 and 20 degrees.

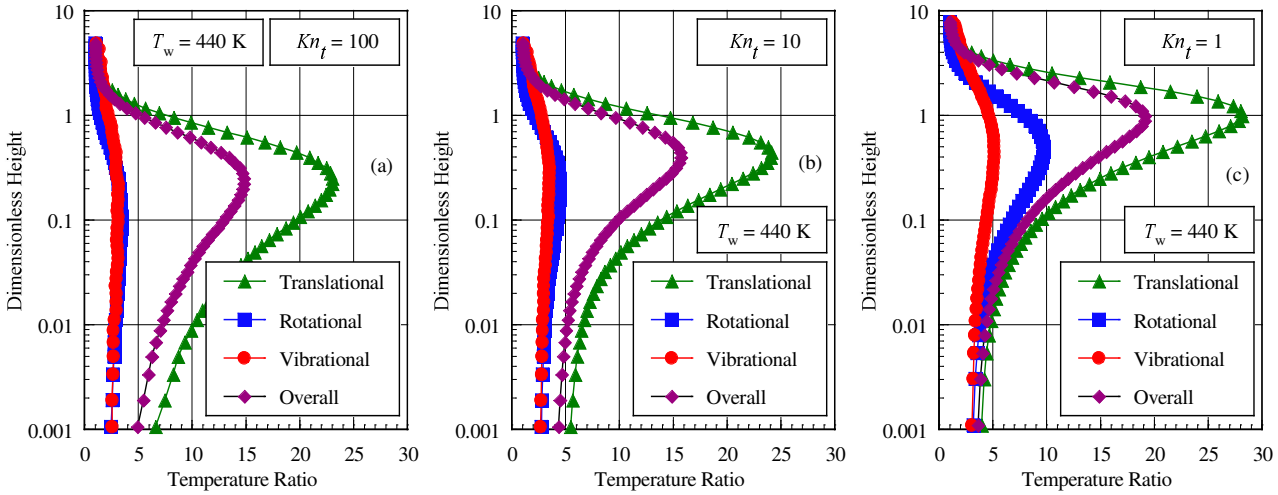

Figure 6: Kinetic temperature (T/T_∞) profiles along the stagnation streamline for leading edge thickness that corresponds to Knudsen number Kn_t of (a) 100, (b) 10 and (c) 1, and wall temperature of 440 K.

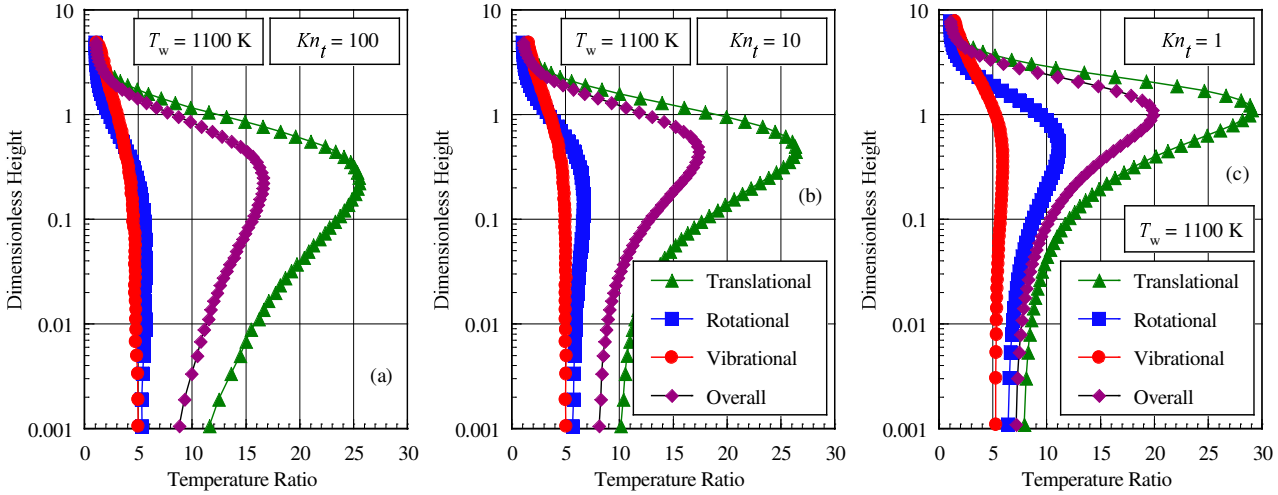

Figure 7: Kinetic temperature (T/T_∞) profiles along the stagnation streamline for leading edge thickness that corresponds to Knudsen number Kn_t of (a) 100, (b) 10 and (c) 1, and wall temperature of 1100 K.

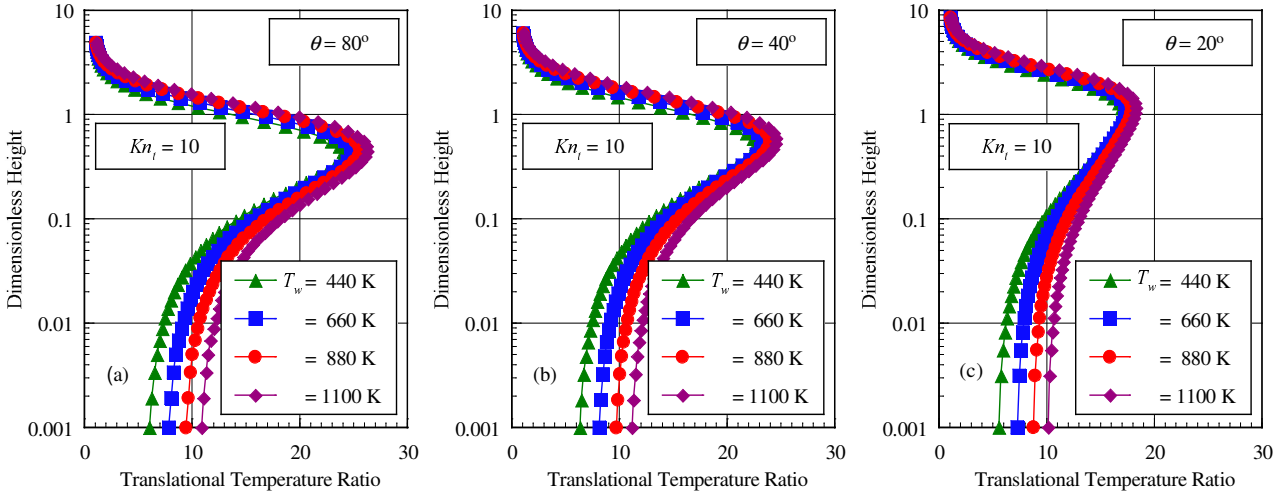

Figure 8: Translational temperature (T_T/T_∞) profiles along the body normal direction as a function of the wall temperature for Knudsen number Kn_t of 10 at afterbody stations that correspond to (a) 80, (b) 40 and (c) 20 degrees.

Figure (8) depicts profiles of translational temperatures at the considered positions normal to the body surface along the η-axis for the Kn_t = 10 case. According to this set of plots, it is observed that the downstream evolution of the flow displays a smearing tendency of the shock wave due to the displacement of the maximum value for the translational temperature. Also, it may be recognized from the translational temperature distribution in Fig. (8) that significant changes in the translational temperature profiles occur within a thin layer adjacent to the body surface for the wall temperature range investigated

In an effort to provide additional information concerning the flowfield structure, dimensionless overall temperature contours, with streamlines patterns, on color maps, are illustrated in Fig. (9) for leading edge thickness that corresponds to Kn_t of 100 and 1 and wall temperature of 440 K. In this figures, X and Y are the length x and height y, respectively, normalized by the freestream mean free path λ_∞.

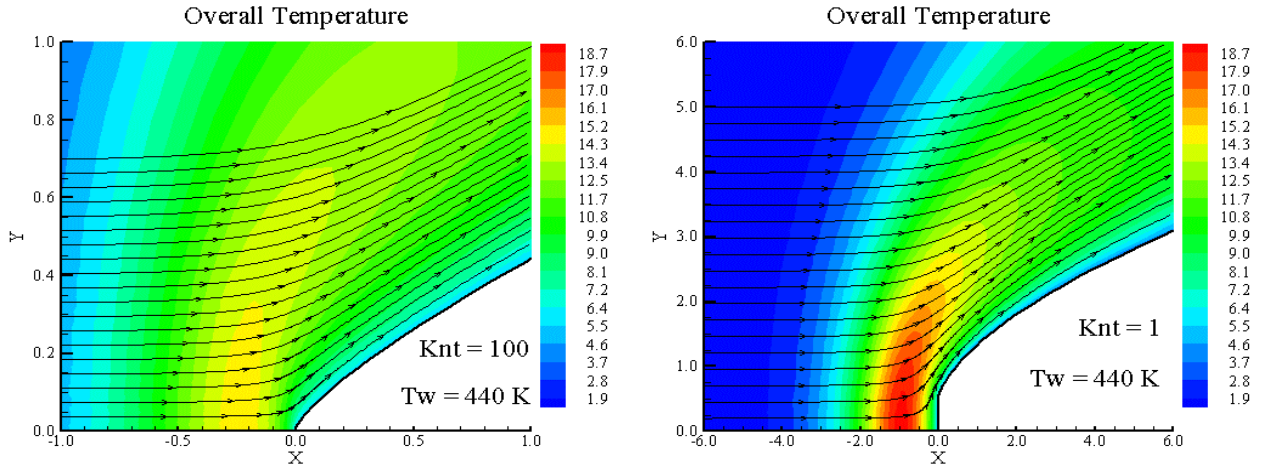

Figure 9: Dimensionless overall temperature (T/T_∞) contours in the vicinity of the leading edge for (a) Kn_t = 100 case and (b) Kn_t = 1 case and wall temperature of 440 K.

4.4. Pressure Profile

The large amount of kinetic energy present in a hypersonic freestream is converted by molecular collisions into high thermal energy surrounding the body and by flow work into increased pressure. In this respect, the stagnation line is a zone of strong compression, where pressure increases from the freestream to the stagnation point due to the shock wave that forms ahead of the leading edges.

Representative pressure profiles along the stagnation streamline are shown as a function of the wall temperature T_w in Figs. (10a), (10b) and (10c) for Kn_t of 100, 10 and 1, respectively. In this set of diagrams, pressure ratio is the pressure p normalized by the freestream pressure p_∞. As can be seen, there is a continuous rise in pressure from the freestream up to the nose of the leading edge. Near the stagnation point, a substantial pressure increase occurs with increasing the leading edge thickness t. It is apparent from these figures that the general shape of the pressure distribution profiles is preserved when the wall temperature is increased from 440 to 1100 K. Pressure is given by the product of the density and the mean value of the square molecular velocity. However, due to the wall temperature rise, density decreases and the translational kinetic temperature, which is associated to the motion of the molecules, increases. As pressure depends on these opposite behaviors, no appreciable changes are observed in the pressure distribution along the stagnation streamline for the wall temperature range investigated.

The extent of the upstream flowfield disturbance for pressure is significantly different from that presented by density. The domain of influence for pressure is higher than that for density and lower than that presented for temperature. Similar to the density, much of the pressure increase in the shock layer occurs after the translational kinetic temperature has reached its postshock value.

Local pressure, expressed as a ratio to the freestream value, for three stations located on the afterbody surface related to the Kn_t = 10 case (t/λ_∞ = 0.1 case) is illustrated in Fig. (11). It is apparent from these profiles that pressure is not affected by the wall temperature rise, as was mentioned earlier. For the station corresponding to 80 deg, Fig. (11a), the pressure variation is in excess of two orders of magnitude for the wall temperature range investigated. In this region, close to the stagnation region, the compression produces a maximum pressure that is around 125 times the freestream value for the wall temperature cases investigated. Due to the expansion along the body surface, the pressure adjacent to the surface decreases to around 60 times the freestream value for wall temperature cases, at the station corresponding to 20 deg, as shown in Fig. (11c), a reduction around of 50% in pressure from station at 80 to 20 degrees.

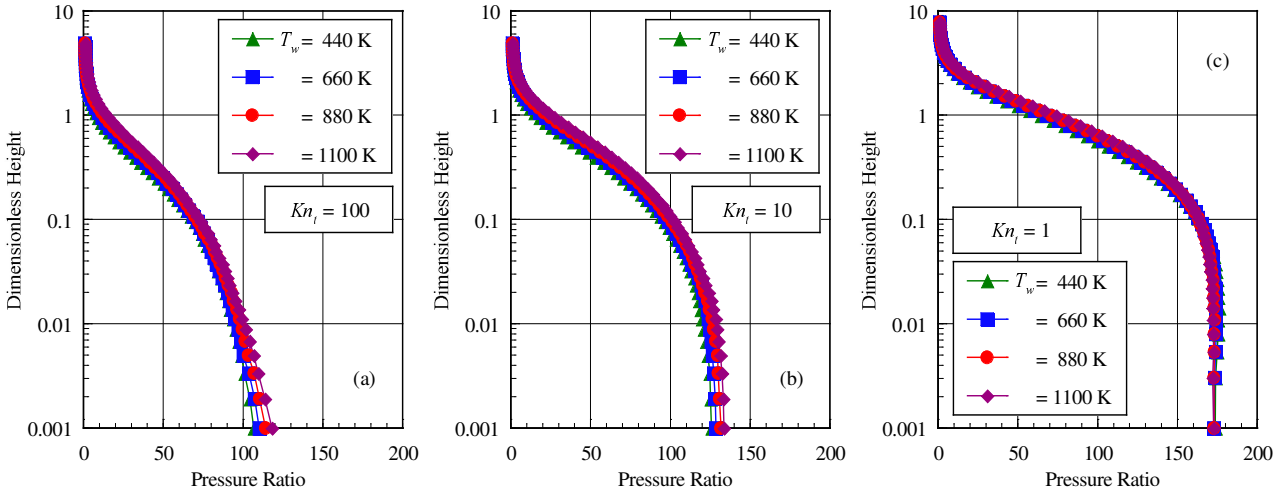

Figure 10: Pressure (p/p_∞) profiles along the stagnation streamline as a function of the wall temperature for leading edge thicknesses that correspond to Knudsen number Kn_l of (a) 100, (b) 10 and (c) 1.

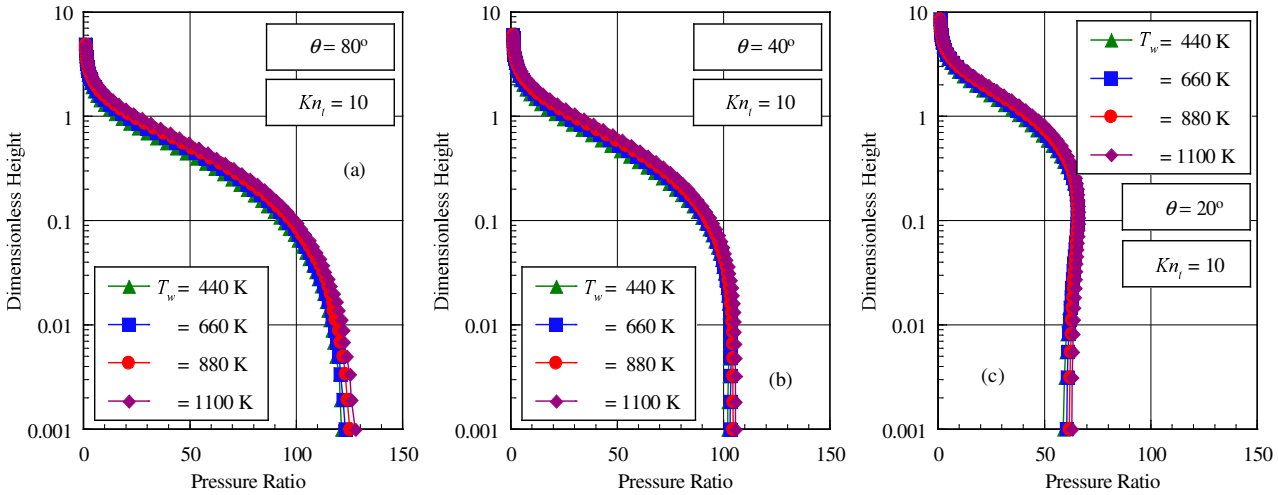

Figure 11: Pressure (p/p_∞) profiles along the body normal direction as a function of the wall temperature for Knudsen number Kn_l of 10 at afterbody stations that correspond to (a) 80, (b) 40 and (c) 20 degrees.

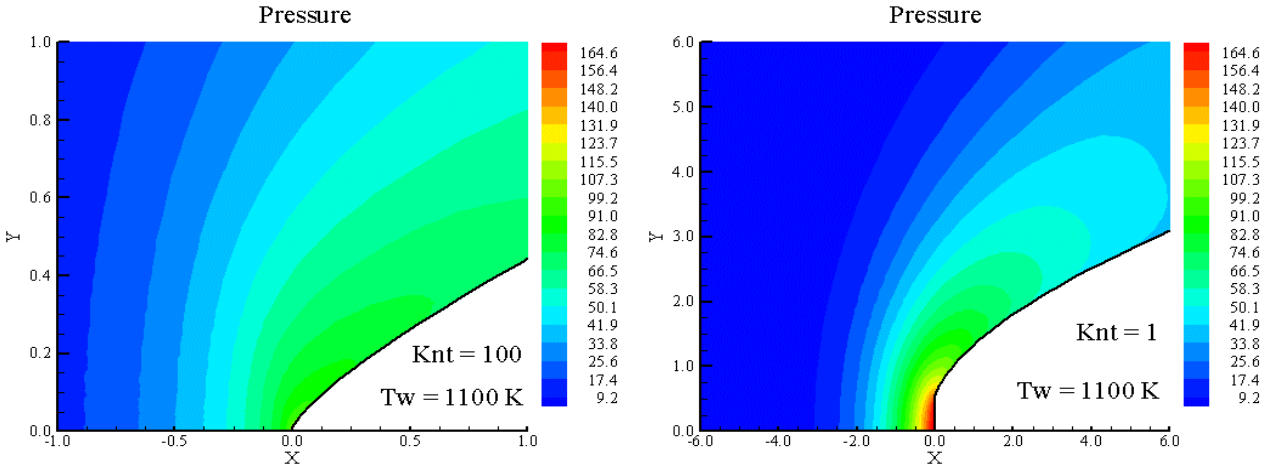

Figure 12: Dimensionless pressure (p/p_∞) contours in the vicinity of the leading edge for Kn_l of (a) 100 and (b) 1, and wall temperature of 1100 K.

In what follows, a critical assessment of the flowfield is provided by Fig. (12), which considers a magnification of the pressure, normalized by the freestream pressure, at the vicinity of the leading edge nose for cases Kn_t of 100 and 1, with wall temperature of 1100 K. This figure confirms that the stagnation region is a zone of strong compression.

5. Concluding Remarks

Computations of a rarefied hypersonic flow on blunt leading edges have been performed by using the Direct Simulation Monte Carlo method. The calculations provided information concerning the nature of the flowfield structure about the primary properties at the vicinity of the nose and immediately adjacent to the body surface for a family of contours composed by a flat nose followed by a highly curved afterbody surface.

Effects of body surface temperature on the velocity, density, pressure, and temperature for a wide range of parameters were investigated. The wall temperature varied from 440 K to 1100 K, set to be from 2 to 5 times the freestream temperature. In addition to that, the leading edge nose thickness ranged from 0.01 to 1 of the freestream mean free path, corresponding thickness Knudsen numbers from 100 to 1. Cases considered in this study covered the hypersonic flow from the transitional flow regime to the free molecular flow regime.

It was found that changes on the shape of the leading edge as well as on the wall temperature disturbed the flowfield far upstream, as compared to the freestream mean free path, and the domain of influence decreased by reducing the nose thickness, as the leading edge became sharp, or by decreasing the wall temperature. Moreover, the extent of the upstream flowfield disturbance is significantly different for each one of the flow properties. The domain of influence for temperature is larger than that observed for pressure and density. Since the extent of the flowfield disturbance is significantly different for each one of the leading edge shapes, this will have important implications in problems that take into account for the gas-phase chemistry and for the gas-surface catalytic activity.

The present document has described an initial investigation of a new class of leading edges for high-altitude low-density flow. Although this investigation has taken into account for a representative number of effects, a number of improvements to a realistic leading edge design is still desirable. The DSMC method has been used to assess the flowfield structure on flat-nose shaped leading edges by considering constant wall temperature. In a realistic design, temperature not only changes along the body surface but also inside the leading edge. In this scenario, a more detailed analysis that includes the conjugate heat transfer problem seems to be challenge.

6. References

Alexander, F. J., Garcia, A. L., and, Alder, B. J., 1998, "Cell Size Dependence of Transport Coefficient in Stochastic Particle Algorithms", Physics of Fluids, Vol. 10, No. 6, pp. 1540-1542.

Alexander, F. J., Garcia, A. L., and, Alder, B. J., 2000, "Erratum: Cell Size Dependence of Transport Coefficient is Stochastic Particle Algorithms", Physics of Fluids, Vol. 12, No. 3, pp. 731-731.

Bird, G. A., 1981, "Monte Carlo Simulation in an Engineering Context", Progress in Astronautics and Aeronautics: Rarefied gas Dynamics, Ed. Sam S. Fisher, Vol. 74, part I, AIAA New York, pp. 239-255.

Bird, G. A., 1989, "Perception of Numerical Method in Rarefied Gasdynamics", Rarefied gas Dynamics: Theoretical and Computational Techniques, Eds. E. P. Muntz, and D. P. Weaver and D. H. Capbell, Vol. 118, Progress in Astronautics and Aeronautics, AIAA, New York, pp. 374-395.

Bird, G. A., 1994, "Molecular Gas Dynamics and the Direct Simulation of Gas Flows", Oxford University Press, Oxford, England, UK.

Borgnakke, C. and Larsen, P. S., 1975, "Statistical Collision Model for Monte Carlo Simulation of Polyatomic Gas Mixture", Journal of computational Physics, Vol. 18, No. 4, pp. 405-420.

Garcia, A. L., and, Wagner, W., 2000, "Time Step Truncation Error in Direct Simulation Monte Carlo", Physics of Fluids, Vol. 12, No. 10, 2000, pp. 2621-2633.

Guo, K. and Liaw, G.-S., 2001, "A Review: Boundary Conditions for the DSMC Method", Proceedings of the 35th AIAA Thermophysics Conference, AIAA Paper 2001-2953, Anaheim, CA, 11-14 June.

Haas, B. L., Fallavollita, M. A., 1994, "Flow Resolution and Domain Influence in Rarefied Hypersonic Blunt-Body Flows", Journal of Thermophysics and Heat Transfer, Vol. 8, No. 4, pp. 751-757.

Hadjiconstantinou, N. G., 2000, "Analysis of Discretization in the Direct Simulation Monte Carlo", Physics of Fluids, Vol. 12, No. 10, pp. 2634-2638.

Liepmann, H. W., Narasimha, R. and Chahine, M., 1964, "Theoretical and Experimental Aspects of the Shock Structure Problem", Proceedings of the 11th International Congress of Applied Mechanics, Ed. H. Gortler, Munich, Germany, pp. 973-979.

Nonweiler, T. R. F., 1959, "Aerodynamic Problems of Manned Space Vehicles", Journal of the Royal Aeronautical Society, Vol. 63, Sept, pp. 521-528.

Reller Jr., J. O., 1957, "Heat Transfer to Blunt Nose Shapes with Laminar Boundary Layers at High Supersonic Speeds", NACA RM-A57FO3a.

Santos, W. F. N., 2003, "Aerodynamic Heating on Blunt Nose Shapes in Rarefied Hypersonic Flow", Proceedings of the 17th International Congress of Mechanical Engineering COBEM 2003, 10-14 Nov, São Paulo, SP, Brazil.